Integrable optical-fiber source of polarization-entangled photon pairs in the telecom band

Xiaoying Li,* Chuang Liang, Kim Fook Lee, Jun Chen, Paul L. Voss, and Prem Kumar
Center for Photonic Communication and Computing, EECS Department, Northwestern University, 2145 Sheridan Road, Evanston, Illinois 60208-3118, USA

(Received 11 January 2006; published 3 May 2006; corrected 8 May 2006)

We demonstrate an optical-fiber-based source of polarization-entangled photon pairs with improved quality and efficiency, which has been integrated with off-the-shelf telecom components and is, therefore, well suited for quantum communication applications in the 1550-nm telecom band. Polarization entanglement is produced by simultaneously pumping a loop of standard dispersion-shifted fiber with two orthogonally polarized pump pulses, one propagating in the clockwise and the other in the counterclockwise direction. We characterize this source by investigating two-photon interference between the generated signal-idler photon pairs under various conditions. The experimental parameters are carefully optimized to maximize the generated photon-pair correlation and to minimize contamination of the entangled photon pairs from extraneously scattered background photons that are produced by the pump pulses for two reasons: (i) spontaneous Raman scattering causes uncorrelated photons to be emitted in the signal and idler bands and (ii) broadening of the pump-pulse spectrum due to self-phase modulation causes pump photons to leak into the signal and idler bands. We obtain two-photon interference with visibility $>90\%$ without subtracting counts caused by the background photons (only dark counts of the detectors are subtracted), when the mean photon number in the signal (idler) channel is about 0.02/pulse, while no interference is observed in direct detection of either the signal or idler photons.

DOI: 10.1103/PhysRevA.73.052301 PACS number(s): 03.67.Hk, 42.50.Dv, 42.65.Lm

I. INTRODUCTION

Entangled photon pairs are a critical resource for realizing various quantum information protocols, such as quantum teleportation, quantum cryptography, database searching, clock synchronization, and quantum computing [1]. Therefore, the efficient generation and distribution of quantum entanglement is of prime importance. The vast majority of entangled-photon sources that are in use in various laboratories around the world today rely on spontaneous parametric down-conversion in $\chi^{(2)}$ crystals [2,3]. However, formidable engineering challenges remain in coupling the entangled photons to standard optical fibers [4–6] for transmission, storage, and manipulation over long distances. Therefore, an efficient and compact entangled photon-pair source created from the fiber itself and emitting entangled photon pairs in the low-loss 1550-nm telecom band is desirable.

Recently, fiber-based sources of entangled photon pairs have been developed by exploiting the $\chi^{(3)}$ (Kerr) nonlinearity of the fiber [7–13]. When the pump wavelength is close to the zero-dispersion wavelength of the fiber, phase matching is achieved and the probability amplitude for inelastic four-photon scattering (FPS) is significantly enhanced. In this process, two pump photons at frequency ω_p scatter through the Kerr nonlinearity of the fiber to create an energy-time-entangled signal and idler photon pair at frequencies ω_s and ω_i, respectively, such that $2\omega_p=\omega_s+\omega_i$. Because of the isotropic nature of the Kerr nonlinearity in fused-silica-glass fiber, the scattered, correlated photon pairs are predominantly copolarized with the pump photons. By coherently adding two such orthogonally polarized FPS processes, polarization entanglement has been created as well [8,9,14]. Using such a fiber-based source, storage and long-distance distribution of polarization entanglement over 50 km of standard single-mode fiber with negligible decoherence has also been recently presented [15], which demonstrates the viability of all-fiber sources for use in quantum memories and quantum logic gates. However, for the polarization-entangled photon-pair source reported in Ref. [8], the relative phase between the two relatively delayed pump pulses needed to be tracked and locked in order to obtain a stable entangled state for the photon pairs, which made the system somewhat complicated. On the other hand, such phase locking is not needed for the source reported in Refs. [9,14], in which a loop of dispersion-shifted fiber (DSF) connected to the two output ports of a polarization beam splitter (PBS) is simultaneously pumped from clockwise (CW) and counterclockwise (CCW) directions with two orthogonally polarized pump pulses. In this scheme, polarization entanglement is produced by a coherent combination of the two FPS processes induced by the CW and CCW propagating pump pulses. More importantly, this setup has two additional advantages: (i) the cross-polarized spontaneous Raman scattering (RS), which is a source of background photons, is automatically suppressed [10] and (ii) the correlated photon pairs generated via FPS from both the CW and CCW pumps emerge in the forward direction, whereas half of the photon pairs generated by each of the two pump pulses are lost in the backward direction in the Sagnac-loop scheme of Ref. [8].

Despite the relative pros and cons of the two schemes [8,9,14], the fiber-based sources demonstrated thus far have been quite inefficient for several reasons. First, the quality of the generated entanglement [8,9] has been limited by the extraneously scattered background photons, whose origin is

*Now at School of Precision Instrument and Opto-electronics Engineering, Tianjin University, Tianjin, 300072, China. Electronic address: xiaoyingli@tju.edu.cn

twofold: (i) spontaneous Raman scattering from the pump pulses causes uncorrelated Stokes (anti-Stokes) photons to be emitted in the signal (idler) bands and (ii) broadening of the pump-pulse spectrum due to self-phase modulation (SPM) in the fiber causes pump photons to leak into the signal and idler bands. Second, the quantum correlation of the photon pairs produced via FPS has not been maximized for lack of careful consideration of the differences in the spectral shape of the pulsed pump and that of the filters used in the signal and idler bands [16]. Finally, the filters used to isolate the pumps [free-space gratings, fiber Bragg gratings (FBG's), and array waveguide gratings (AWG's)] have been quite lossy, resulting in a low rate for the generated entangled photon pairs.

In this paper, using a scheme similar to that reported in Refs. [9,14], we demonstrate an optical-fiber source of polarization entangled photon pairs with improved quality and efficiency, which has been integrated with off-the-shelf telecom components and is, therefore, well suited for quantum communication applications in the 1550-nm telecom band. The quality of the source is improved by carefully optimizing the experimental parameters in order to suppress the contamination due to RS and SPM of the pump pulses and to maximize the correlation of the signal-idler photon pairs produced via FPS. The efficiency of the source is improved by using cascaded wave-division-multiplexing (WDM) filters (CWDMF) that not only isolate the pump with lesser loss but also improve the correlation of the generated signal-idler photon pairs because of their squarish (super-Gaussian) shape. We characterize the source by experimentally investigating two-photon interference (TPI) between the generated signal-idler photon pairs under various conditions. TPI with visibility $>90\%$ is obtained without subtracting counts caused by the background photons (only dark counts of the detectors are subtracted), while no interference is observed in direct detection of either the signal or idler photons. All four Bell states can be created with our source.

II. EXPERIMENTAL DETAILS

A schematic of our experimental setup is shown in Fig. 1(a). Signal and idler photon pairs at wavelengths of 1533.9 nm and 1543.5 nm, respectively, are produced via the FPS process in a 300-m piece of DSF having a zero-dispersion wavelength at $\lambda_0=1538\pm2$ nm. Pump pulses with a central wavelength of 1538.7 nm are decomposed into horizontally and vertically polarized components P_H and P_V, respectively, by use of a polarization beam splitter (PBS) P_1 and launched into the DSF. P_H propagates CW in the DSF producing correlated photon pairs $|H\rangle_s|H\rangle_i$, whereas P_V propagates CCW producing $|V\rangle_s|V\rangle_i$. A fiber polarization controller (FPC) is used with the DSF to compensate the birefringence introduced by bending and coiling of the fiber on a spool. It takes about 2 μs for a pump pulse to propagate through the loop formed by the DSF and P_1. For such a short time period, the pump pulses P_H and P_V, launched simultaneously into the loop in CW and CCW directions, can be viewed as propagating along a frozen path, irrespective of the local environmental perturbations, acoustic and thermal,

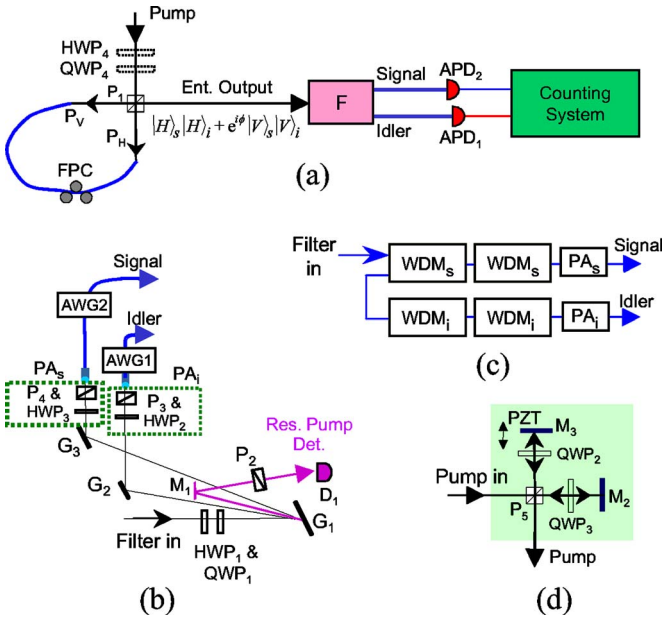

FIG. 1. (Color online) (a) Experimental setup. (b) Configuration of the filter F composed of a double-grating filter followed by an AWG (DGFAWG). (c) Configuration of the filter F composed of two cascaded WDM filters (CWDMF). (d) Schematic of the pumping scheme. P_1-P_5, polarization beam splitters; F, filter; G_1-G_3, diffraction gratings; AWG, array-waveguide grating; M_1-M_5, mirrors; FPC, fiber polarization controller; QWP, quarter-wave plate; HWP, half-wave plate; PA_s and PA_i, polarization analyzers.

which occur on millisecond time scales. The correlated wave packets $|H\rangle_s|H\rangle_i$ and $|V\rangle_s|V\rangle_i$ also see a similar frozen path and are coherently superimposed upon arrival at P_1. For a photon pair emerging at the output port of P_1, there is no way to determine whether it was created by the CW (horizontally polarized) or CCW (vertically polarized) pulse [see Fig. 1(a)]. This indistinguishability gives rise to polarization entanglement, resulting in the output state $|\Psi\rangle=|H\rangle_s|H\rangle_i+e^{i\phi}|V\rangle_s|V\rangle_i$, where ϕ is the relative phase difference between the wave packets $|H\rangle_s|H\rangle_i$ and $|V\rangle_s|V\rangle_i$, which is determined by the details of phase matching in the DSF and the phase accumulated by the signal, idler, and pump photons in propagating along their respective directions. In our experiment $\phi=2\phi_p$, where ϕ_p is the relative phase between P_H and P_V. This is because in FPS the sum of the phases of the signal and idler photon pairs equals the sum of the phases of the two pump photons and the propagation phases accumulated in the CW and CCW directions cancel out.

This source can produce all four polarization-entangled Bell states. When $\phi_p=0,\frac{\pi}{2}$, the states $|\Psi^{\pm}\rangle=|H\rangle_s|H\rangle_i\pm|V\rangle_s|V\rangle_i$ are created. In our setup, $\phi_p=0$ is obtained by launching a linearly polarized pump pulse and then using a half-wave plate (HWP_4) to rotate the polarization direction to 45°relative to P_1. Additionally, when a quarter-wave plate (QWP_4) with its axis parallel to P_1 is placed right after HWP_4, then $\phi_p=\frac{\pi}{2}$ is achieved. The other two Bell states $|\Phi^{\pm}\rangle=|H\rangle_s|V\rangle_i\pm|V\rangle_s|H\rangle_i$ can be prepared by inserting a properly oriented HWP in the idler channel. Nonmaximally

entangled pure states having an arbitrary degree of polarization entanglement can also be created with this setup by choosing the two pump pulses (P_H and P_V) to have unequal powers, which can be accomplished by rotating the HWP_4.

Polarization entanglement is measured by using polarization analyzers (PA's) [each composed of a rotatable half-wave plate (HWP) and a PBS; see Fig. 1(b)] in the signal and idler channels. For the state $|\Psi\rangle=|H\rangle_s|H\rangle_i+e^{i2\phi_p}|V\rangle_s|V\rangle_i$, when the polarization analyzers in the signal and idler channels are set to θ_1 and θ_2, respectively, the single-count probability for the signal and idler photons is $R_j=\frac{1}{2}\eta_j\alpha$ $(j=1,2)$. The coincidence-count probability R_{12} can then be expressed as $R_{12}=\frac{1}{2}\xi\eta_1\eta_2\alpha[\cos^2\theta_1\cos^2\theta_2+\sin^2\theta_1\sin^2\theta_2+2\cos(2\phi_p)\sin\theta_1\cos\theta_1\sin\theta_2\cos\theta_2]$, where $\eta_j(j=1,2)$ is the total detection efficiency, θ_j $(j=1,2)$ is the angle of the PA in each channel, α is the photon-pair production rate, and ξ is a coefficient determined by the spectrum of the pump pulse and that of the filters in the signal and idler bands.

To detect the scattered photon pairs with good signal to noise, an isolation of the pump photons in excess of 100 dB is required. Because of the nonzero response time of the Kerr nonlinearity [17], there are actually three kinds of photons that emerge from the output port [see Fig. 1(a)]: (i) entangled signal and idler photon pairs produced by the FPS process, (ii) photons in the signal and idler bands produced by the RS process, and (iii) residual pump photons that leak into the signal and idler bands because of spectral broadening caused by SPM. Since the Kerr nonlinearity is relatively weak, for 300 m of DSF only about 0.1 photons on average are scattered by a typical 5-ps-duration pump pulse containing approximately 10^7 photons. We achieve the required isolation by sending all the photons emerging from the output port through a specially made filter F, which is realized in two ways. In one configuration (DGFAWG), F is composed of a double-grating filter (DGF), providing an isolation greater than 75 dB [7], followed by array-waveguide gratings (AWG's) (Wavesplitter, model WAM-10-40-G), providing isolation greater than 40 dB [17], wherein the passband of the DGFAWG is determined by both the passband of the DGF and that of the channel used in the AWG. The second configuration of F (CWDMF) is composed of two cascaded WDM filters (JDSU, models DWS-2F2863P90 and DWS-2F3353P90), each one providing an isolation greater than 70 dB in each channel. The two configurations are schematically shown in Figs. 1(b) and 1(c), respectively, and their transmission spectra are plotted in Fig. 2(a). Each passband of DGFAWG fits a Gaussian function well with a full width at half maximum (FWHM) of 0.4 nm, as shown in Fig. 2(b). In contrast, each passband of CWDMF is well fitted with a fourth-order super-Gaussian function having a FWHM of 1 nm, as shown in Fig. 2(c). The dynamic range of the spectra shown in Fig. 2 is limited by the intrinsic noise of the optical spectrum analyzer (OSA) used to make the measurements. The total isolation to out-of-band pump photons provided by the filter F in both configurations is greater than 110 dB.

The pump is a 5-ps-duration mode-locked pulse train with a repetition rate of 75.3 MHz, obtained by spatially dispersing the output of an optical parametric oscillator (OPO) (Coherent, model Mira-OPO) with a diffraction grating [8]. To achieve the required power, the pump pulses are then amplified by an erbium-doped fiber amplifier (EDFA). Photons at the signal and idler wavelengths—from the OPO that leak

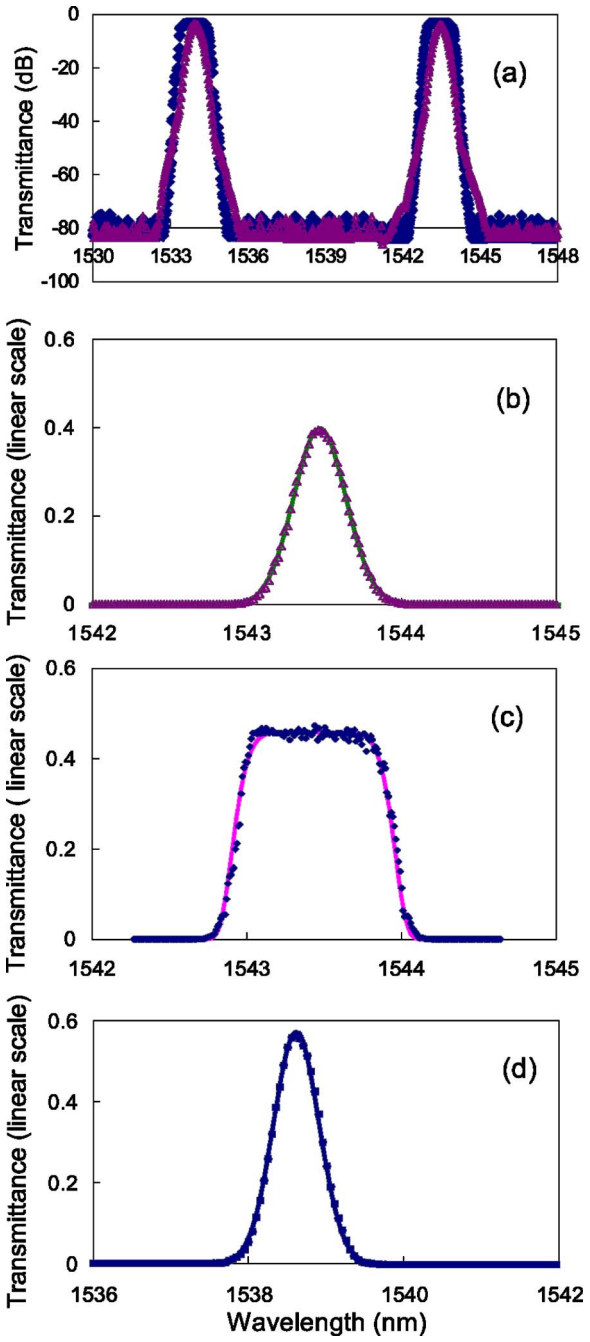

FIG. 2. (Color online) Passband spectra for the various filters used in our setup. Solid curves are fits to the data. (a) Transmission spectra for the DGFAWG filter (triangles) and the CWDMF filter (diamonds). (b) One passband of the DGFAWG fitted with a Gaussian function $f(\lambda)=0.4\exp\left[-\frac{1}{2}\left(\frac{\lambda-1543.5}{0.17}\right)^2\right]$, where the FWHM is about 0.4 nm. (c) One passband of the CWDMF fitted with a super-Gaussian function $f(\lambda)=0.46\exp\left[-\frac{1}{2}\left(\frac{\lambda-1543.5}{0.49}\right)^{2m}\right]$, $m=4.1$, where the FWHM is about 1.0 nm. (d) Filtered spectrum of the pump pulse (squares) fitted with a Gaussian function $f(\lambda)=0.55\exp\left[-\frac{1}{2}\left(\frac{\lambda-1538.7}{0.33}\right)^2\right]$, where the FWHM is about 0.8 nm.

through the spectral-dispersion optics and from the amplified spontaneous emission in the EDFA—are suppressed by passing the pump through a 1-nm-bandwidth tunable filter (Newport, model TBF-1550-1.0). In our experiment, the spectrum of pump pulses is well fitted with a Gaussian function of 0.8 nm FWHM, as shown in Fig. 2(d).

The signal and idler photons are detected with photon counters consisting of InGaAs/InP avalanche photodiodes (APDs) (Epitaxx, model EPM 239BA) operated in a gated-Geiger mode [7]. The 1-ns-wide gate pulses arrive at a rate of 588 kHz, which is 1/128 of the repetition rate of the pump pulses. The quantum efficiency for one detector is 25%, for the other is 20%. The total detection efficiencies for the signal and idler photons are about 3.5% and 2.8% (10% and 8% with CWDMF), respectively, when the efficiencies of the DSF (80%), DGFAWG ($\simeq$20%) [CWDMF ($\simeq$80%)], and other transmission components (about 80%) are included. For the CWDMF, an efficiency of $\simeq$80% should also be included when PA's are inserted.

III. RESULTS

Our first measurement for characterizing the polarization correlation of the source involves setting both PA's at 45°and slowly scanning the relative phase ϕ_p between P_H and P_V while observing the photon counts, both singles and coincidences. Phase scanning is accomplished by adding separate free-space propagation paths for P_H and P_V with use of a PBS (P_5), two quarter-wave plates (QWP_2 and QWP_3), and two mirrors (M_2 and M_3) [see Fig. 1(d)]. M_3 is mounted on a piezoelectric-transducer- (PZT-) driven translation stage, which allows us to precisely adjust the free-space path difference and hence the relative phase ϕ_p. For this measurement, the pump powers for both P_H and P_V are about 0.3 mW and the DGFAWG is used to reject the pump. During the measurement, the phase ϕ_p is simultaneously monitored by tapping off the rejected pump with a mirror M_1 placed after the grating G_1 and measuring it with a low-bandwidth photodetector D_1 placed behind a polarizer P_2. This arrangement is equivalent to monitoring one output port of the polarization interferometer formed between P_1 and P_2 [see Fig. 1(b)]. The fringe contrast of the interfering P_H and P_V pulses is maximized by appropriately adjusting the position of M_3 (by applying an appropriate voltage on the PZT) and the orientations of HWP_1 and QWP_1. This ensures that P_H and P_V arrive at P_1 simultaneously and that the rejected P_H and P_V are oriented at ±45° relative to the axis of P_2. The results are presented in Fig. 3(a), where one sees good interference in the coincidence counts whereas no interference is observed in the single counts. In plotting the coincidence counts only the dark counts of the detectors have been subtracted. By fitting the plotted coincidence counts with a cosine function, we obtain a TPI visibility of 71%. These results are obtained at a production rate of 0.1 photons/pulse, which is deduced from the detected single counts and among them the photon-pair production rate is about 0.07 pairs/pulse [19].

The output of D_1 is plotted in Fig. 3(b), which when compared with the TPI result shown in Fig. 3(a) clearly shows

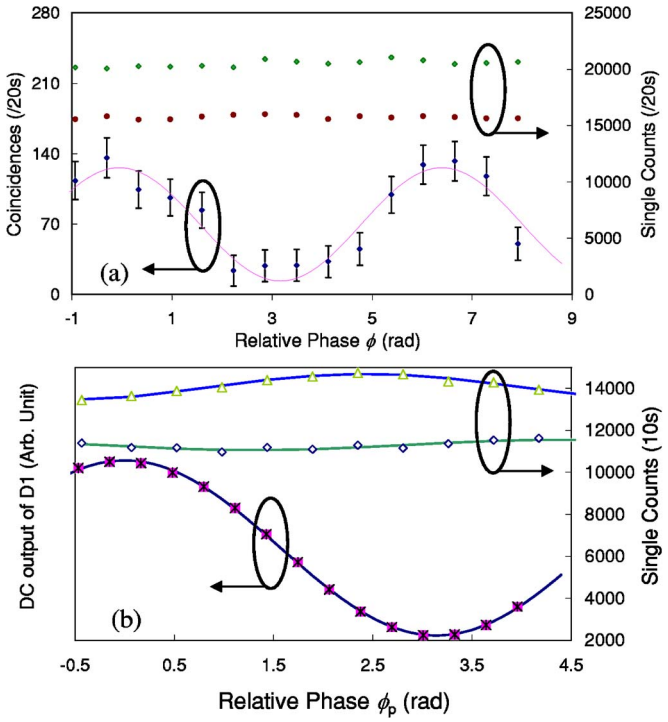

FIG. 3. (Color online) Measurement of polarization entanglement as the relative phase ϕ_p is varied with both the PA's set at 45°relative to the verticle. Solid curves are best fits. (a) Coincidence counts and single counts detected over 20 s versus $\phi=2\phi_p$ when the pump powers for both P_H and P_V are about 0.3 mW. (b) Left ordinate: plot of the output from detector D_1 (squares) showing one-photon interference in the rejected pump pulses with twice the fringe spacing as in (a). Right ordinate: single counts in signal (triangles) and idler (diamonds) bands detected over 10 s versus ϕ_p when the pump powers for both P_H and P_V are about 0.4 mW. The fitting curve for the signal (idler) is phase shifted by about 2 rad behind (ahead) that for the pump.

that the relative phase ϕ between the wave packets $|H\rangle_s|H\rangle_i$ and $|V\rangle_s|V\rangle_i$ is twice the pump phase ϕ_p, i.e., $\phi=2\phi_p$. It is worth noting that when the pump power is higher, slight variations also begin to appear in the single counts, with the variation in signal band being more than that in idler band. This is also shown in Fig. 3(b), which was obtained with pump powers for both P_H and P_V to be about 0.4 mW. Fitting the single counts with a cosine function, we find that the periodicity in the single-count variations is the same as that of the pump, but the phases are different. For the signal counts the fringe maximum occurs behind that of the pump by about 2 rad, while for the idler counts it is ahead of the pump maximum by the same amount of phase shift. We see a similar behavior upon further increasing the pump power; only the magnitude of the variations in the single counts is increased.

We believe that the SPM of the pump is responsible for the observed variations in the single counts. Although the isolation provided by the filter F (DGFAWG for the data in Fig. 3) is good enough to effectively reject the pump photons

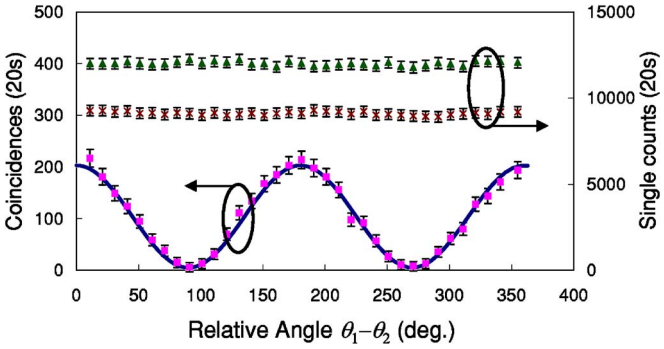

FIG. 4. (Color online) Coincidence counts and single counts detected over 20 s as the analyzer angle in the idler channel is varied while keeping the analyzer angle in the signal channel fixed at 45° relative to the vertical. The solid curve is a best fit, yielding a TPI visibility of 92%.

at the central wavelength, the SPM-induced spectral broadening of the pump pulses at higher powers causes pump photons at the signal and idler passband frequencies to leak through the filter F. These leakage photons give rise to first-order interference observed in the single counts.

One way to reduce the influence of the SPM is to increase the detuning of the signal band from the pump. However, the detuning needs to be decreased to suppress the RS in the DSF [10]. Therefore, we improve the quality of our source by optimizing the system parameters such that the RS and SPM are suppressed while the correlation of the photon pairs produced by the FPS is maximized, in accordance with our measurements of these effects in Refs. [10,16,17]. Thus, we replace the Gaussian-shaped DGFAWG with a FWHM of 0.4 nm by the super-Gaussian-shaped CWDMF with a FWHM of 1 nm. Additionally, because the loss of each WDM used to construct the CWDMF is only about 0.5 dB, the efficiency of the source is significantly improved.

With the optimized configuration of the system, we measure the TPI again with pump powers of P_H and P_V at about 0.05 mW each. Blocking the light reflected from M_2 and adjusting HWP_4 to 22.5°relative to P_1 (see Fig. 1), we obtain a pump which is linearly polarized with an angle of 45° relative to P_1. In making the measurement, the QWP_4 is either taken out or oriented with its axis parallel to the linearly polarized pump. In this way we set $\phi_p=0$ so that the two-particle quantum state emerging from the output port is $|\Psi\rangle^+=|H\rangle_s|H\rangle_i+|V\rangle_s|V\rangle_i$. TPI measurements are made by fixing the PA in the signal channel at 45°while rotating the PA in the idler channel. The results are shown in Fig. 4, wherein only the dark counts of the detectors have been subtracted. These results are obtained for a production rate of about 0.02 photons/pulse (deduced from the single-count measurements), among which the photon-pair production rate is about 0.006 pairs/pulse [19], corresponding to a pair emission rate of 7×10^4 correlated photon pairs per second from the output tips of the signal and idler fibers. Clearly, we observe much improved TPI, while the single counts in both the channels remain constant. Again by fitting the coincidence counts with a cosine function, a TPI visibility of 92% is obtained.

For comparison, we increase the pump powers of P_H and P_V to about 0.15 mW and make the TPI measurement again. Under this condition, we obtain a deduced production rate of about 0.13 photons/pulse, among which the photon-pair production rate is about 0.07 pairs/pulse [19]. Thus, at the same photon-pair production rate as in Fig. 3, the RS in this case is larger. And yet, we observe TPI with a higher visibility of about 78% than the visibility of 71% in Fig. 3. This increase in visibility is because the correlation of the detected photons produced via FPS is maximized by using a super-Gaussian filter such as the CWDMF with a wider and flat passband.

IV. CONCLUSIONS

We have demonstrated a high-quality source of polarization-entangled photon pairs by using a counterpropagating scheme in which an optical-fiber loop is simultaneously pumped with orthogonally polarized pulses in clockwise and counterclockwise directions. We produce high-quality photon pairs by carefully optimizing the system parameters in order to suppress the negative effects of Raman scattering and self-phase modulation of the pump pulses and to maximize the photon-pair correlation through the four-photon scattering process. We have characterized the source by investigating two-photon interference between the generated signal-idler photon pairs under various experimental conditions. At a production rate of about 0.02 photons/pulse in the signal (idler) channel, among which the photon-pair production rate is about 0.006 pairs/pulse, two-photon interference with visibility $>90\%$ is obtained without subtracting counts caused by the background photons (only dark counts of the detectors are subtracted), while no interference is observed in direct detection of either the signal or the idler photons. All four Bell states can be created with this source, which is integrated with off-the-shelf telecom components and is, therefore, well suited for quantum communication applications in the 1550-nm telecom band. Additionally, the production rate can be dramatically increased by pumping the DSF with a mode-locked fiber laser operating at a repetition rate above 10 GHz, which will lead to over 10^7 correlated photon pairs per second being emitted from the output tips of the signal and idler fibers. Moreover, the free-space components of the present setup can be replaced with commercially available fiber-spliced components, which would make the source very compact and easily integrable into the existing fiber network.

The main advantage of our fiber-based source of polarization-entangled photon pairs is that such a source can be easily spliced into a transmission fiber with negligible loss for long-distance quantum communications. In contrast, coupling of the entangled photons generated by a $\chi^{(2)}$-crystal source to a transmission fiber is very delicate [4–6,18]. Another advantage of the fiber source over its crystal counterpart is the excellent single-model purity, which is highly desirable for realizing quantum networks involving multiple entangling operations. Besides, it is possible to wavelength multiplex several different entangled channels carved from the broadband parametric spectrum of FPS by utilizing recently developed multiplexing and demultimplexing devices.

The main disadvantage of the fiber source is the existence of RS. However, the visibility of TPI is expected to be improved to over 98% by cooling the fiber to further suppress the RS. Therefore, we believe that the integrable fiber source of entangled photon pairs presented in this paper will be a promising tool for developing technologies for quantum information processing.

ACKNOWLEDGMENTS

We would like to thank Dr. Jay E. Sharping for useful discussions. This work was supported in part by the DOD Multidisciplinary University Research Initiative (MURI) Program administered by the Army Research Office under Grant DAAD19-00-1-0177.

[1] C. H. Bennett and P. W. Shor, IEEE Trans. Inf. Theory **44**, 2724 (1998).
[2] D. C. Burnham and D. L. Weinberg, Phys. Rev. Lett. **25**, 84 (1970).
[3] P. G. Kwiat, K. Mattle, H. Weinfurter, A. Zeilinger, A. V. Sergienko, and Y. H. Shih, Phys. Rev. Lett. **75**, 4337 (1995).
[4] F. A. Bovino, P. Varisco, A. M. Colla, G. Castagnoli, G. D. Giuseppe, and A. V. Sergienko, Opt. Commun. **227**, 343 (2003).
[5] S. Castelletto, I. P. Degiovanni, A. Migdall, and M. Ware, New J. Phys. **6**, 87 (2004).
[6] R. Andrews, E. R. Pike, and S. Sarkar, Opt. Express **12**, 3264 (2004).
[7] M. Fiorentino, P. L. Voss, J. E. Sharping, and P. Kumar, IEEE Photonics Technol. Lett. **14**, 983 (2002).
[8] X. Li, P. L. Voss, J. E. Sharping, and P. Kumar, Phys. Rev. Lett. **94**, 053601 (2005).
[9] H. Takesue and K. Inoue, Phys. Rev. A **70**, 031802(R) (2004).
[10] X. Li, J. Chen, P. L. Voss, J. Sharping, and P. Kumar, Opt. Express **12**, 3737 (2004).
[11] J. G. Rarity, J. Fulconis, J. Duligall, W. J. Wadsworth, and P. S. J. Russell, Opt. Express **13**, 534 (2005).
[12] J. E. Sharping, J. Chen, X. Li, and P. Kumar, Opt. Express **12**, 3086 (2004).
[13] J. Fan, A. Dogariu, and L. J. Wang, Opt. Lett. **30**, 1530 (2005).
[14] P. Kumar, M. Fiorentino, P. L. Voss, and J. E. Sharping, U.S. Patent No. 6,897,434 (2005).
[15] X. Li, P. L. Voss, J. Chen, J. E. Sharping, and P. Kumar, Opt. Lett. **30**, 1201 (2005).
[16] J. Chen, X. Li, and P. Kumar, Phys. Rev. A **72**, 033801 (2005).
[17] X. Li, P. L. Voss, J. Chen, K. F. Lee, and P. Kumar, Opt. Express **13**, 2236 (2005).
[18] T. B. Pittman, B. C. Jacobs, and J. D. Franson, Opt. Commun. **246**, 545 (2005).
[19] The photon-pair production rate is deduced from the ratio between the detected photons produced via FPS and those produced via RS at the corresponding pump power. This ratio can be obtained by measuring the single counts in the signal (idler) channel, $N_{s(i)}$, as a function of the number of pump photons per pulse, N_p, and by fitting the measured data with $N_{s(i)}=s_1N_p+s_2N_p^2$, where s_1 and s_2 are the linear and quadratic scattering coefficients, which respectively determine the strengths of the RS and the FPS. Detailed information can be found in Fig. 5 of Ref. [10]